Liquefaction susceptibility underneath a large storage tank: a CPT based methodology

Greef, J. de, Lengkeek, H.J., Brunetti, M., Besseling, F.
Witteveen+Bos Consulting Engineers, Deventer, The Netherlands

ABSTRACT
Accurate prediction of the onset of liquefaction and the consequential soil behaviour in terms of strength and stiffness is in general a difficult topic. In particular when high static shear stresses are involved, as is the case near the edges of a shallow founded large storage tank, reliable results obtained from coupled finite element methods (FEM) are lacking.

In this study a practical approach is presented to evaluate the liquefaction susceptibility underneath a shallow founded large storage tank using Cone Penetration Test (CPT) data that is obtained prior to installation of the storage tank. The CPT based liquefaction triggering procedure by Idriss & Boulanger (2008) is adopted. Where deemed helpful, some additional thought is given to the topics of static shear stress effects and the estimation of excess pore pressures. In essence the triggering procedure predicts the liquefaction susceptibility at one specific point, but in spreadsheet analyses it is often applied to a 1D vertical soil column. From an axisymmetrical FEM model including the storage tank, all stresses in the subsoil are converted to square grid data points which allows for a 2D spreadsheet-based liquefaction triggering analysis. With conditional formatting various zones in the subsoil with a different susceptibility to liquefaction are in this way identified graphically.

The consequential strength and stiffness reductions in these zones are fed back to the FEM model to establish various seismically induced ground deformation scenarios. By coupling these scenarios to critical structural failure states of the storage tank, the overall tank redundancy to seismic loading can be improved effectively.

1 INTRODUCTION

Utility firms or in general companies with a large social responsibility often stand to benefit from, or even are obliged to perform quantitative risk assessments (QRA). As the consequences of failure increase, the accepted probability of failure decreases. Chemical plants and oil storage facilities are examples of industrial sites with the obligation to perform a QRA.

Confronted with the task to quantitatively assess the probability of failure due to an earthquake the obvious initial question is: how can an earthquake lead to failure of a storage tank? Both structural and geotechnical failure could ultimately lead to a loss of containment scenario. This study focuses only on structural failure that is caused by seismically induced ground deformations.

The development of numerical models that accurately predict the onset of liquefaction and the consequential soil behavior in terms of strength and stiffness, is still ongoing. In particular when high static shear stresses are involved, as is the case near the edges of a shallow founded large storage tank, reliable results obtained from coupled FEM analysis are lacking.

In this study a practical approach is presented to evaluate the liquefaction susceptibility underneath a shallow founded large storage tank using CPT data that is obtained prior to installation of the storage tank. Although this evaluation is difficult as it is deterministically, where possible suggestions are provided that could ultimately lead to a fully probabilistic approach.

2 METHODOLOGY

The outline of the methodology is presented in Figure 1. The CPT data used for the analysis is obtained prior to the installation of the tank. By using multiple correlations all relevant parameters of the Hardening Soil Small Strain (HSS) constitutive model as implemented in Plaxis finite element code, are determined.

After parameter verification multiple site response analyses are performed and the stresses in the subsoil are determined from Plaxis. Using these stresses a liquefaction analysis is performed, resulting in estimations of the excess pore pressure ratios. These result in shear strength reductions, which are fed back in the FEM model to analyze the seismically induced ground deformations which may ultimately lead to structural failure.

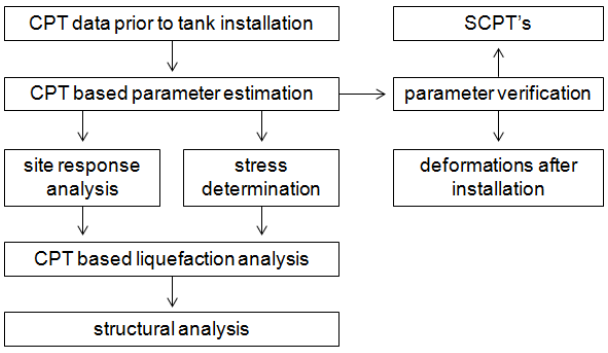

Figure 1. Methodology outline

3 CPT BASED PARAMETER ESTIMATION

Prior to installation of the storage tank 17 CPTs were taken that have a circular spatial distribution: one in the center, four at a distance of half the radius and twelve near the current edge of the storage tank.

3.1 Constitutive model

Many different constitutive finite element models are available. For this study the HSS model in the finite element code Plaxis is adopted as it has proven to perform well in both static and dynamic loading conditions. Moreover, the authors have experience with parameter estimation for this model based on CPT data.

The HSS constitutive model is able to represent the actual hysteretic soil behaviour in cyclic loading and therefore can be very well used for seismic geotechnical analyses. The hysteretic damping is controlled by stiffness parameters G_0^{ref}, E_{ur}^{ref} and $\gamma_{0.7}$. By proper selection of these parameters the HSS constitutive model is very well capable of representing the actual cyclic stress strain response of different soil types.

However, if these parameters are derived to optimize the model performance in dynamic loading conditions it should be verified that a consistent set of parameters is derived that can also capture static performance. If necessary stiffness parameters E_{oed}^{ref} and E_{50}^{ref} can be adjusted to some extent to improve the model performance for larger strains in static conditions, without undermining the model performance dynamically.

The available CPT data is analyzed to identify different soil strata and establish the subsoil characterization of the storage tank site. By using multiple correlations basic parameters such as unit weights, relative densities and shear wave velocities are estimated. Using these all relevant parameters of the HSS model are determined.

3.2 Verification of static parameters

For the shallow founded storage tanks the parameters and model performance are assessed by reproducing the soil consolidation behaviour of the storage tank at the stage of filling and water testing.

With this verification step it is evaluated that a consistent set of parameters is derived that is able to reproduce the actual stress strain behaviour of the soil layers present at the site and thereby can reproduce the storage tank foundation performance.

3.3 Verification of dynamic soil parameters

The dynamic soil parameters obtained from the CPT data are partially verified by comparing a combination of existing correlations (Robertson (2009a), Hardin (1978), and Mayne (2007)) with SCPT measurement data that is obtained on site.

An exemplary result of this comparison is presented in Figure 2. The comparison leads the authors to believe that the in-situ shear wave velocity V_s and consequently the small-strain stiffness G_0 are approximated with reasonable accuracy.

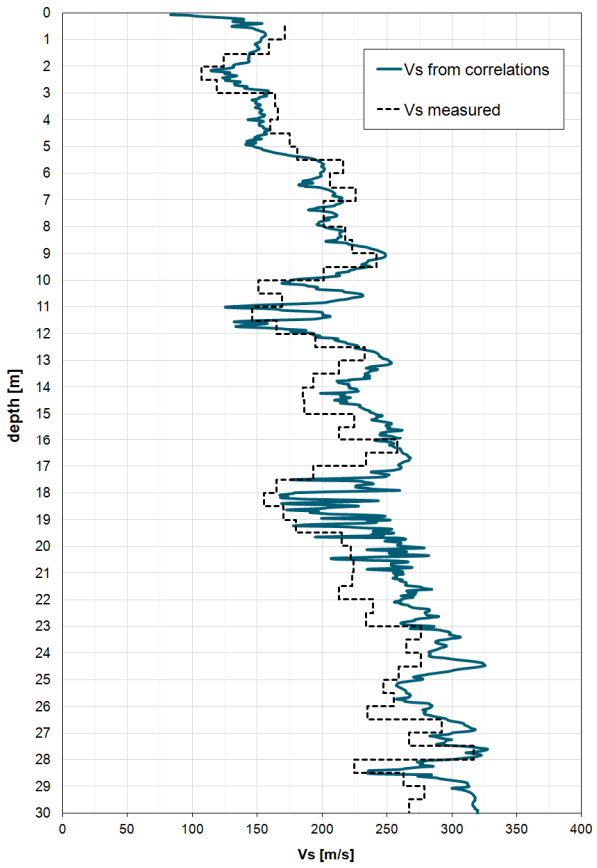

Figure 2. CPT based correlation compared with SCPT

4 2D STRESS CONDITIONS

For the structural analysis of the tank an axisymmetric FEM model of the storage tank is set up to reduce calculation efforts. This will be explained in chapter 6.

The model of the subsoil including the filled tank is presented in Figure 3. The stresses in the subsoil are obtained from a fine-meshed version of this model.

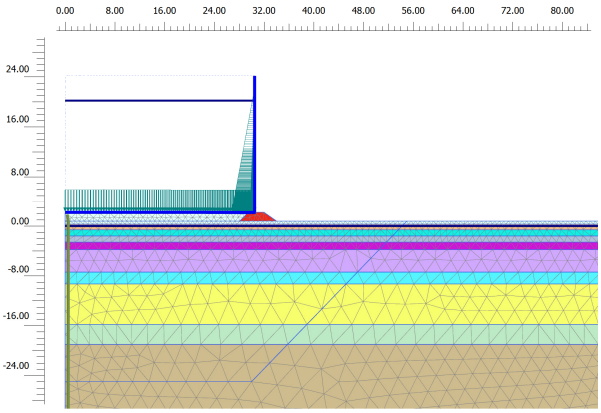

Figure 3. Axisymmetric FEM model of the subsoil (meters)

Due to the shape of the elements in the FEM model, the stresses cannot be imported directly in a spreadsheet based format to perform the liquefaction analysis. The data from the triangularly distributed nodes is therefore transformed to equidistant 25 cm square nodes by using interpolation software. An example of the transformation result is presented in Figure 4 which shows the static shear stress ratios α near the footing of the storage tank in a conditionally formatted spreadsheet.

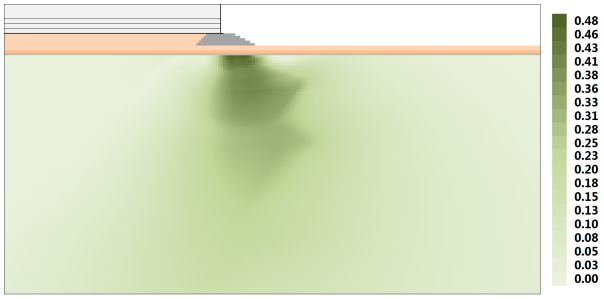

Figure 4. Static shear ratio α underneath the storage tank

5 CPT BASED LIQUEFACTION ANALYSIS

For the CPT based liquefaction analysis the method by Idriss & Boulanger (2008) is adopted. The advantage of this method is that it allows for the explicit formulation of additional overburden and static shear effects through respectively the overburden correction factor K_σ and the static shear stress correction factor K_α.

5.1 Probabilistic CRR curves

The liquefaction triggering procedure by Idriss & Boulanger (2008) is a deterministic method. To obtain an expected value of FS_{liq} rather than a deterministic value, the definition of the CRR curve is modified. This is done by implementing a variable exceedance probability P_L similar to the probabilistic CRR formulation presented in Boulanger & Idriss (2014) with $\sigma_{ln(R)}$ being equal to 0.20. Herein q_{c1Ncs} is the clean sand equivalent normalized cone tip resistance.

$$CRR_{M_w=7.5\,;\,\sigma'_v=100\,kPa\,;\,\alpha=0} = \exp\left(\frac{qc1Ncs}{540} + \left(\frac{qc1Ncs}{67}\right)^2 - \left(\frac{qc1Ncs}{80}\right)^3 + \left(\frac{qc1Ncs}{114}\right)^4 - 2.8 + \sigma_{\ln(R)} \cdot \Phi^{-1}(P_L)\right) \quad [1]$$

The result of this procedure is presented in Figure 5 which shows the CRR curves for three different probabilities of exceedance (PoE): 16% (deterministic), 50% and 85%.

For the purpose of comparison between liquefaction triggering methods, at the same levels of exceedance probability the CRR curves from Boulanger & Idriss (2014) and Robertson (2009b) are presented in Figure 5 too, the latter based on the work by Ku et al. (2012).

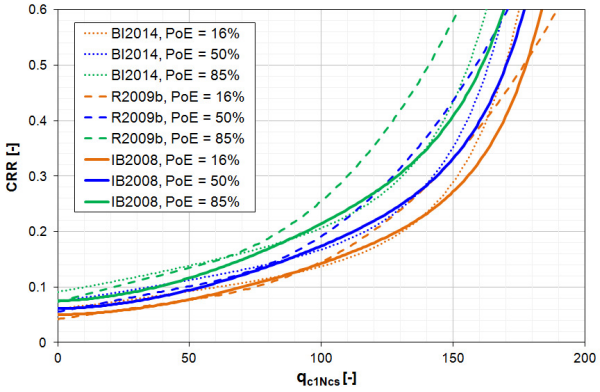

Figure 5. CRR curves at various liquefaction exceedance probabilities

5.2 Static shear stress effects

The effect of static shear stresses on the liquefaction susceptibility is not described easily as the complex formulation to account for its effect by Boulanger (2003) emphasizes. The curves in Figure 6 represent the value of K_α at different values of the relative state parameter ξ_R.

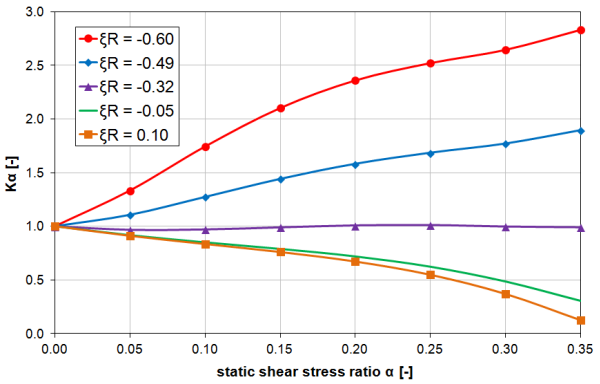

Figure 6. Relationship between K_α and α

As can be observed from the K_α-α relationship, the effect of static shear stresses on the liquefaction susceptibility appears to be absent for values of the relative state parameter ξ_R close to -0.32. The relative state parameter is defined by Boulanger (2003) as the difference between the critical state relative density $D_{R;CS}$ and the apparent relative density D_R. Therein the relative dilatancy index framework by Bolton (1986) is adopted.

The solid curve in Figure 7 represents the critical state line by Bolton (1986) under static loading conditions. For combinations of the apparent relative density and isotropic stress above this curve, the large strain behavior is contractive. Below this curve the behavior is dilative.

With a vertical offset of 0.32 the dotted curve is obtained, which can be seen to represent the apparent relative density at which K_α = 0 in agreement with the results from Figure 6. Below this curve the behavior is

dilative (lower liquefaction susceptibility) and above this curve contractive (higher liquefaction susceptibility). The strain level at which a sample is said to liquefy is typically 3% and the isotropic stress levels on which the offset of 0.32 is determined ranges from about 100 to 1,600 kPa.

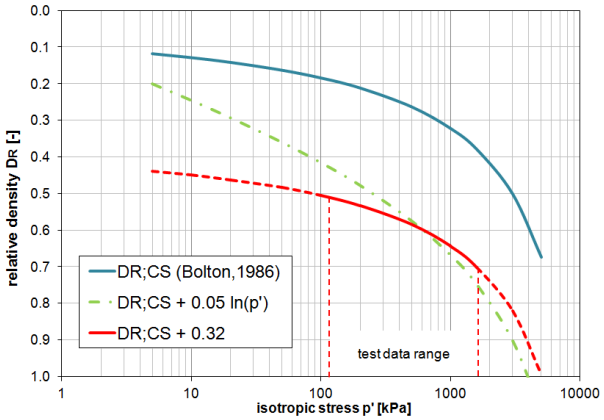

Figure 7. Critical state and $K_\alpha = 0$ curves

In between the solid and dotted curves there appears to be a transition zone, where under static shear loading conditions dilative behavior is observed, while under cyclic shear loading conditions the behavior appears to be contractive. From preliminary numerical soil test simulations the authors found that the height of the transition zone, or vertical offset, appears to be stress dependent. This is particularly true in the lower confining stress range, where test data is absent.

The dash-dotted curve in Figure 7 (see Eq. [2]) is only illustrative. Rather than being a constant, the vertical offset is now logarithmically dependent on the effective isotropic stress p'. Within the range of stress levels that are present within the test data the difference between the curves is limited.

$$D_{R;K_\alpha=0} = D_{R;CS} + 0.05\ln(p') \qquad [2]$$

The upward shift of the dash-dotted curve implies that at low stress levels dilative behavior is expected at lower relative densities. Regarding the K_α-α relationship in Figure 6, it means the ξ_R = -0.32 curve will shift upwards. Unfortunately it is unknown how much the other curves in the same figure will shift. In this study therefore the vertical offset equal to 0.32 will be maintained. Generally speaking it is expected that at lower isotropic stress levels, static shear stresses will lead to lower liquefaction susceptibility than is currently assumed.

The result of the contemplation above in the K_α-ξ_R plane is shown in Figure 8. In this figure the value of K_α is presented for varying relative state parameters. By adopting a stress-dependent relation such as Eq. [2] the transition zone becomes narrower at lower confining stress levels.

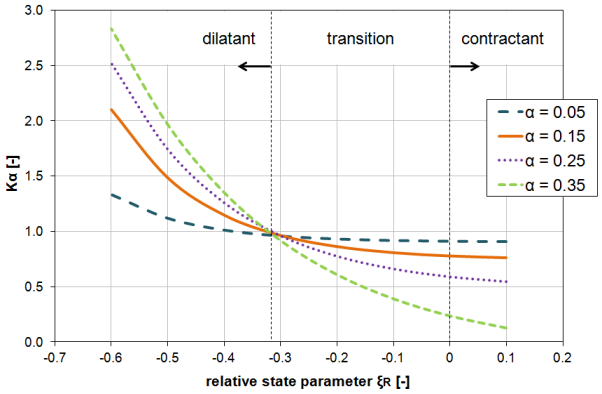

Figure 8. K_α relation in the K_α - ξ_R plane

5.3 Excess pore pressures

In order to assess the liquefaction induced deformations the strength- and stiffness reduction of the subsoil due to (partial) liquefaction is implemented through the excess pore pressure ratio r_u. To obtain the value of r_u two empirical equations that are briefly elaborated below, are combined.

$$\frac{N_A}{N_B} = \left(\frac{\tau_A}{\tau_B}\right)^{-1/b} \quad \rightarrow \quad \frac{N}{N_{liq}} = \left(\frac{CRR}{CSR}\right)^{-1/b} \qquad [3]$$

Eq. [3] describes the linear relationship between the logarithm of the shear stress amplitude ratio (τ_A/τ_B) and the logarithm of the equivalent cycle ratio N_A/N_B. If τ_B (CSR) represents the actual stress level, then N_B (N_{liq}) equivalent cycles are required to induce liquefaction at this stress level. If the actual number of cycles is N_A (N), then the stress level required to induce liquefaction at this number of cycles is equal to τ_A (CRR). The cycle ratio N/N_{liq} can thus be related directly to FS_{liq}.

The value of b depends on soil type and state. Tokimatsu & Yoshimi (1982) find typical values of about 0.20 for sand. When adopting the triggering procedure by Idriss & Boulanger (2008) a value of 0.34 may be adopted as this value of b is consistent with the maximum value of the magnitude scaling factor MSF_{max} equal to 1.8.

Boulanger & Idriss (2015) have drastically modified the formulation of the magnitude scaling factor and introduced a direct dependency on q_{c1Ncs}. The value of b is implicitly present in this formulation. It can be back calculated directly from CPT by using a relation between the equivalent number of cycles N_{cyc} and b similar to the formulation used in the regression analysis by Kishida & Tsai (2013). In Figure 9 the result of Eq. [4] is shown that is obtained by performing this back calculation. Note that b approaches 0.15 at q_{c1Ncs} = 0 due to the fact that the minimum value of MSF_{max} is equal to 1.09.

$$q_{c1Ncs} = 185.4 \cdot \sqrt[3]{\left[\tfrac{4}{3}\exp(3.09 + 1.79\ln b)\right]^b - 1} \qquad [4]$$

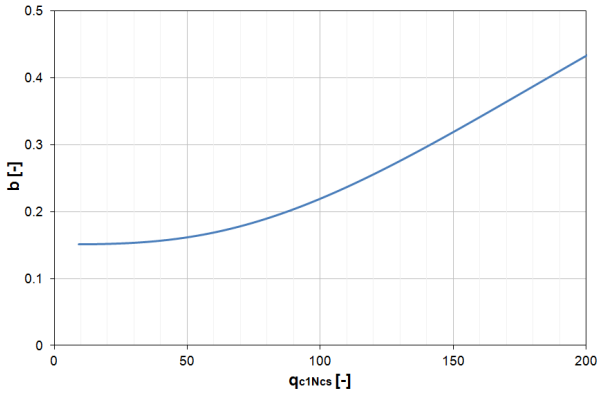

Figure 9. Relation between q_{c1Ncs} and b

Eq. [5] describes the dependency of the pore pressure ratio r_u on the cycle ratio. The formulation is obtained from Booker et al. (1976) and a herein a typical value for θ is said to be 0.7 for all soil types. They also note that this value is actually soil dependent but no further detail is given on how different soil types affect the parameter.

$$r_u = \frac{2}{\pi}\arcsin\left(\left(\frac{N}{N_{liq}}\right)^{1/2\theta}\right) \qquad [5]$$

Idriss & Boulanger (2008) appear to use a value of θ equal to 1.0 as this provides a perfect match for the curve that is presented in Figure 10 below. Although soil dependency of θ is not addressed, the strong dependency of the static shear stress ratio α on the pore pressure build-up is described. To be able to calculate r_u in a spreadsheet format the r_u-N/N_{liq} curve at α = 0.3 is approximated by Eq. [6]. For values of α in between 0.0 and 0.3 a weighted average of Eq. [5] and Eq. [6] is used which results in the curves presented in Figure 10.

$$r_u = \left(\frac{N}{N_{liq}}\right)^{0.185} \qquad [6]$$

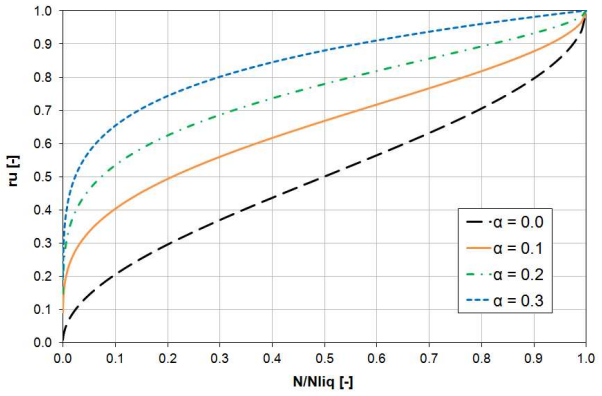

Figure 10. Dependency of pore pressure build-up on α

By combining Eq. [3] with Eq. [5] the curves in Figure 11 are obtained, which are valid for level ground conditions where α = 0. The difference in r_u values for varying values of b is significant, but the impact of the value of b on MSF_{max} can be far more dominant, particularly for earthquakes with relatively low magnitudes.

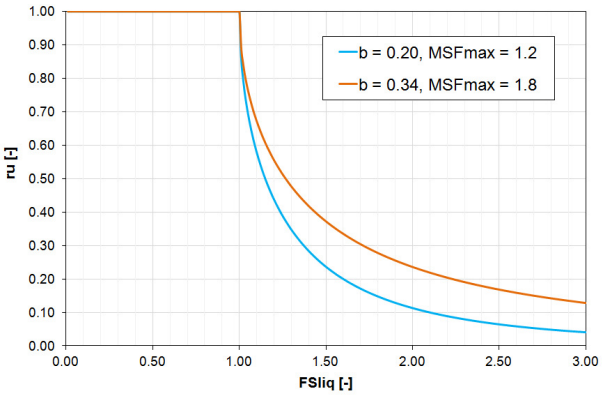

Figure 11. Relation between FS_{liq} and r_u (at α = 0)

Having set a definition for r_u the 2D spreadsheet based liquefaction analysis can be completed. For a typical CPT and peak ground acceleration the result of the analysis is presented in Figure 12. It shows the excess pore pressure ratios r_u underneath the storage tank. It can be seen clearly that liquefaction susceptibility is largest in two superficial soil layers. Underneath the tank the soil is less likely to liquefy than under free-field conditions due to the adjusted ratio between total and effective stresses that defines the cyclic stress ratio CSR. The liquefaction susceptibility of the soil layers that were already most likely to liquefy increases significantly due to the presence of static shear stresses near the edge of the tank.

Figure 12. Excess pore pressures below the storage tank

The final step towards the structural analysis is relating the r_u values to reduced strength and stiffness parameters that can be implemented in Plaxis.

The strength- and stiffness reductions calculated from Eq. [7] and Eq. [8] are implemented to different zones that are depicted from the liquefaction analysis, of which Figure 12 gives an example. The subscripts *red* and *0* respectively stand for reduced and initial.

$$\varphi'_{red} = \operatorname{atan}\left((1 - r_u) \cdot \tan \varphi'_0\right) \quad [7]$$

$$E_{red} = \sqrt{(1 - r_u)} \cdot E_0 \quad [8]$$

6 STRUCTURAL ANALYSIS

Geotechnical failure due to liquefaction in itself does not imply a loss of containment scenario. However, due to liquefaction induced (geotechnical) deformations a critical structural failure state may develop that does cause a loss of containment. This is captured in the analysis by means of the following approach:

- Various seismically induced deformation scenarios are determined. These deformations consist of three components that need to be accounted for: reduced bearing capacity deformations, squeezing effects and post-liquefaction settlements. The former two are accounted for in the FEM model, the latter is estimated by adopting the framework by Yoshimine et al. (2006). The different scenarios account for the effects of the spatial distribution of the deformations around the tank.
- With a structural finite element model the performance of the tank with respect to the relevant structural failure mechanisms is defined for the various liquefaction induced deformation scenarios.
- For each deformation scenario a critical structural failure state is established with a corresponding critical deformation level.
- By this means liquefaction induced deformations are coupled to critical structural failure states. This coupling is eventually represented graphically by fragility curves.

This approach enables the effective assessment of the weakest elements of the structure, given a liquefaction potential risk. Moreover, the results of such analyses clearly indicate which structural elements or detailing should be improved in order to improve the overall tank redundancy to seismic loading.

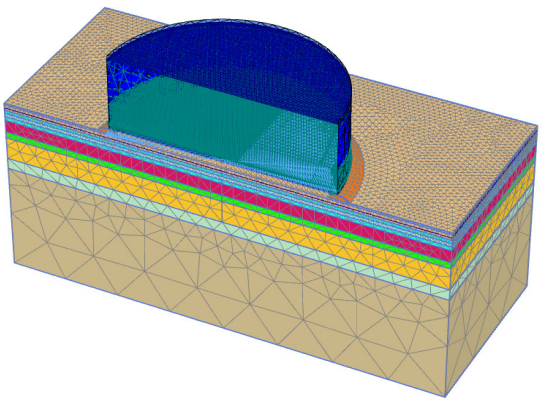

Figure 13. Structural model in Plaxis 3D

The stability analyses are initially performed using a 3D model of the storage tank in Plaxis. In order to reduce the computational effort, advantage is taken of the symmetry of the structure as presented in Figure 13.

For the given subsoil conditions and seismic loads, local subsoil deformations near the edges of the tank appear to be the dominant cause of structural failure. Moreover, for the type of structural failure that is most likely to occur, it is insignificant whether the subsoil deformations are only local or occur simultaneously on different locations underneath the storage tank.

Disregarding the overturning moment caused by sloshing and thus assessing the stability after the earthquake, a comparison of the 3D model is made with a 2D axisymmetrical model of the tank. This comparison yielded satisfactory results (see Figure 14 and Figure 15), which means calculation effort and time can be reduced significantly. In turn this allows for a more thorough sensitivity analysis of subsoil and seismic load variations.

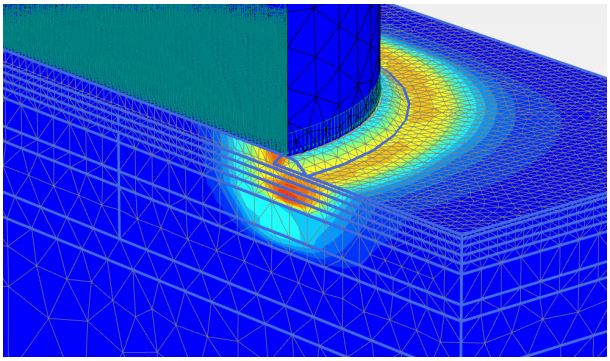

Figure 14. Deformations near the tank edge in 3D model

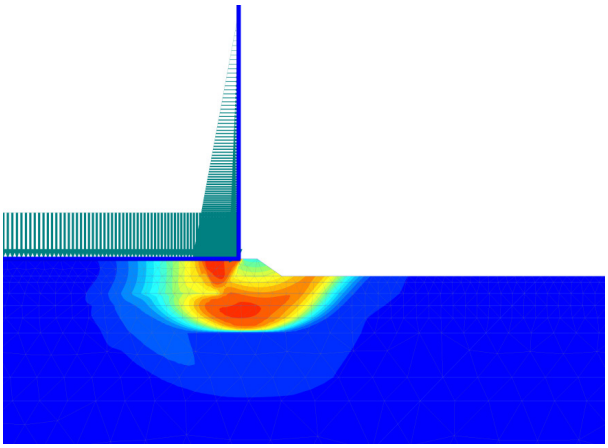

Figure 15. Deformations near the tank edge in 2D model

By using an updated mesh procedure vertical displacements can be calculated up to a magnitude of several decimeters at which geotechnical equilibrium is no longer reached. Although dependent on the structural detailing, this typically exceeds the structural capacity and is thus sufficient to quantify the redundancy of the system.

7 CONCLUSIONS

In this study an approach is presented to analyze the seismically induced ground deformations underneath a large storage tank, using only CPT data obtained prior to installation of the tank.

By analyzing the available measurement data of both the filling and water testing stage and from several SCPTs taken on site, confidence is gained that the used constitutive model and derived parameters provide accurate results.

As the static shear stresses are very high, the effect of static shear stresses on the liquefaction susceptibility appears to be very significant. The set of available equations to estimate this effect is derived at relatively high confining stresses, especially compared to the situation of interest in this study. It is therefore recommended that test data should be expanded to the lower confining stress range.

By obtaining and transforming stresses in the subsoil from an axisymmetrical FEM model, the liquefaction triggering procedure by Idriss & Boulanger (2008) that is usually performed in a 1D vertical soil column is now performed in two dimensions. Although it is still a simplified method, insight is provided graphically in the effect of high isotropic and static shear stresses on the liquefaction susceptibility underneath the storage tank.

Using the results from the liquefaction analysis, the structural redundancy of the tank to ground deformations is analyzed by combining critical structural failure states with seismically induced ground deformation scenarios.

8 REFERENCES

Booker, J.R., Rahman, S.M., Bolton Seed, H. 1976. *GADFLEA: A Computer Program for the Analysis of Pore Pressure* Generation *and Dissipation During Cyclic or Earthquake Loading*, University of California, Berkeley, California, USA.

Bolton, M.D. 1986. *The strength and diltancy of sands*, Géotechnique 36(1): 65-78.

Boulanger, R.W. 2003. *Relating K_α to Relative State Parameter Index*, J. Geotech. Geoenviron. Eng., ASCE, 129(8): 770-773.

Boulanger, R.W. and Idriss, I.M. 2014. *CPT and SPT Based Liquefaction Triggering Procedures*, Report No. UCD/CGM-14/01, University of California, Davis, California, USA

Boulanger, R.W. and Idriss, I.M. 2015. *Magnitude scaling factors in liquefaction triggering procedures*, Soil Dynamics and Earthquake Engineering, Elsevier, 79: 296-303.

Hardin, B.O. 1978. *The Nature of Stress-Strain Behavior for Soils*, Proceedings on the Speciality Conference on Earthquake Engineering and Soil Dynamics, ASCE.

Idriss, I.M. and Boulanger, R.W. 2008. *Soil Liquefaction During* Earthquakes, Earthquake Engineering Research Institute (EERI), Oakland, California, USA.

Kishida, T. and Tsai, C. 2013. *Seismic Demand on the Liquefaction Potential with Equivalent Number of Cycles for Probabilistic Seismic Hazard Analysis*, DOI: 10.1061/(ASCE)GT.1943-5606.0001033, J. Geotech. Geoenviron. Eng., ASCE

Ku, C., Juang, C., Chang, C., Ching, J. 2012. *Probabilistic version of the Robertson and Wride method for liquefaction evaluation: development and application*, Can. Geotech. J., 49: 27-44.

Mayne, P.W. 2007. *NCHRP Synthesis 368: Cone Penetration Test*, Transportation Research Board, National Academies Press, Washington DC, USA.

Robertson, P.K. 2009a. *Interpretation of cone penetration test - a unified approach*, Can. Geotech. J., 46: 1337-1335.

Robertson, P.K. 2009b. *Performance based earthquake design using the CPT*, DOI: 10.1201/NOE0415556149.ch1, Proc. IS-Tokyo 2009, 3-20.

Tokimatsu, K. and Yoshimi, Y. 1982. *Liquefaction of Sand due to Multidirectional Cyclic Shear*, Soil and Foundations, Japanese Society of Soil Mechanics and Foundation Engineering, 22(3): 126-130.

Yoshimine, M., Nishizaki, H., Amano, K., Hosono, Y. 2006. *Flow deformation of liquefied sand under constant shear load and its application to analysis of flow slide of finite slope*, Soil Dynamics and Earthquake Engineering, Elsevier, 26: 253-264.